Pressure–Volume–Derived Ventricular Energetics Across Mechanical Circulatory Support Strategies in Cardiogenic Shock

Jorge A. Ortega-Hernández,*† Luca Baldetti,‡ Guglielmo Gallone,§¶ Giulio Cacioli,‖ Pier Paolo Bocchino,§ Héctor González-Pacheco,* Luis Amezcua-Guerra,# Mariagiulia Festi,‡ Francesca Pirone,‡ Francesco Calvo,‡ Stefania Sacchi,‡ Marina Pieri,‡ Silvia Ajello,‡ Simone Frea,§ Marta Pasquero,¶ Fabio Sbaraglia,‖ Gaetano Maria De Ferrari,§¶ Giampaolo Luzi,‖ Rashidi Springall,# Antonio Loforte,§¶ Jaime Hernández-Montfort,** Anna Mara Scandroglio,‡ and Alexandra Arias-Mendoza*

Bedside pressure–flow variables in cardiogenic shock (CS) incompletely characterize ventricular energetics and coupling. We prospectively derived bedside pressure–volume (PV) loop surrogates from paired pulmonary artery catheter and echocardiographic data in 68 patients (263 paired assessments) with acute myocardial infarction–related CS (AMI-CS) or heart failure–related CS (HF-CS) during microaxial support, intra-aortic balloon pump (IABP) support, or medical therapy. In AMI-CS with microaxial support, arterial elastance decreased (−1.22 mm Hg/ml) with improved coupling (ventriculoarterial coupling [VAC] −1.42), stroke work increased (+140 mm Hg·ml), and pressure–volume area declined (PVA −103 mm Hg·ml), yielding an efficiency rise from ~32% to ~40%, suggesting unloading. In HF-CS, microaxial support reduced elastance modestly (−0.35) with probable efficiency gain (+5%) but heterogeneous PVA changes. In AMI-CS treated with IABP, coupling improved (VAC −0.42) with modest energetic augmentation, whereas HF-CS showed pressure and energy amplification (end-systolic pressure +23.9 mm Hg; PVA +220.6 mm Hg ·ml). Without mechanical support, AMI-CS demonstrated reduced elastance and pressure, while HF-CS exhibited ventricular dilation (end-diastolic volume [EDV]/end-systolic volume ESV increase) with higher energetic demand. Pressure–volume–derived metrics identify device-specific energetic signatures not fully captured by conventional hemodynamic assessment and may provide mechanistic insight into ventricular unloading strategies; validation against conductance catheter–derived PV measurements remains warranted. *ASAIO Journal* 2026; XX:XX–XX

https://links.lww.com/ASAIO/B954

Key Words cardiogenic shock, mechanical circulatory support, ventricular energetics, pressure–volume analysis, microaxial pump, intra-aortic balloon pump, pressure–volume loop, pulmonary artery catheter

Cardiogenic shock (CS) involves impaired cardiac output and organ hypoperfusion, often treated with vasoactive agents and mechanical support (tMCS). Improvements in pressure–flow variables may not reduce myocardial demand or unload the ventricle. Pressure–volume (PV) analysis integrates ventriculoarterial coupling and energetics, revealing trade-offs not shown by standard metrics (Figure 1).[1]

Direct PV-loop acquisition with conductance catheters is the standard for ventricular mechanics but is limited in clinical use due to cost, technical complexity, and feasibility.[1,2] Pressure–volume assessment is rarely available during CS management, when understanding therapy effects is most relevant. This creates a need for practical bedside PV surrogates.

Pulmonary artery catheterization (PAC) and echocardiography are widely used in CS to phenotype shock, guide escalation/de-escalation of support, and monitor response to therapy.[3] While PAC offers precise intracardiac and pulmonary pressures and flow estimates, echocardiography provides structural and systolic function data.[4] Integrating these complementary bedside measurements enables estimation of quantitative PV-loop surrogates without introducing additional invasive instrumentation.

The purpose of this study was to derive bedside PV-loop surrogates from paired PAC and echocardiographic measurements and to characterize device- and etiology-specific hemodynamic response patterns in CS across acute myocardial infarction–related CS (AMI-CS) and heart failure–related CS (HF-CS) treated with microaxial flow pump support (mAFP), intra-aortic balloon pump support (IABP), or medical therapy alone.

Coronary Care Unit, *Instituto Nacional de Cardiología Ignacio Chávez, Ciudad De México, Mexico; †Programa de maestría y doctorado en ciencias médicas y odontológicas de la Salud, Universidad nacional Autónoma de México, Ciudad De México, Mexico; ‡Cardiac Intensive Care Unit, IRCCS San Raffaele Scientific Institute, Milan, Italy; §Division of Cardiology, "Città della Salute e della Scienza" Hospital, Turin, Italy; ¶Department of Medical Sciences, University of Turin, Turin, Italy; ‖Cardiac Surgery and Heart Transplant Unit, Azienda Ospedaliera San Camillo Forlanini, Rome, Italy; #Instituto Nacional de Cardiología Ignacio Chávez, Immunology, Ciudad De México, Mexico; and **Advanced Heart Failure and Recovery Program for Central Texas Baylor Scott & White Health, Round Rock, Texas.

Submitted for consideration February 2026; accepted for publication in revised form April 2026.

Disclosure: The authors have no conflicts of interest to report.

Supplemental digital content is available for this article. Direct URL citations appear in the printed text, and links to the digital files are provided in the HTML and PDF versions of this article on the journal's Web site (www.asaiojournal.com).

Correspondence: Jorge A Ortega-Hernández, Coronary Care Unit, Instituto Nacional de Cardiología Ignacio Chávez, Juan Badiano 1, Sección XVI, Tlalpan, Mexico City 14080, Mexico. E-mail: jorgeoh1992@gmail.com.

DOI: 10.1097/MAT.0000000000002737

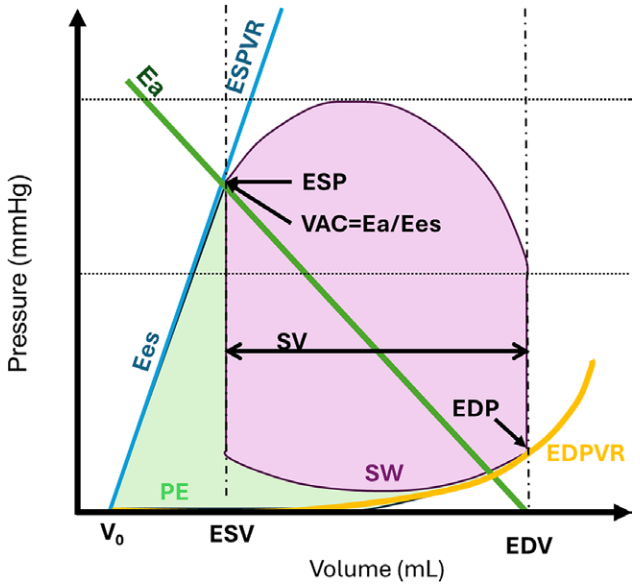

Figure 1. Pressure–volume loop surrogates and ventricular arterial coupling. The diagram illustrates the PV loop surrogates, depicting key hemodynamic relationships. ESPVR (blue line) represents ventricular contractility, while EDPVR (yellow curve) defines passive filling properties. Ea (green line) reflects afterload, and (R)Ees (blue line) indicates ventricular stiffness. SW (purple area) represents the external mechanical work done by the ventricle, whereas PE (green area) is the stored energy. VAC is defined as Ea/(R)Ees and represents the interaction between cardiac function and vascular load. SV is the horizontal distance between the end-diastolic and end-systolic volumes. Ea, arterial elastance; EDPVR, end-diastolic pressure–volume relationship; Ees, end-systolic elastance; ESPVR, end-systolic pressure–volume relationship; PE, potential energy; PV, pressure–volume; SV, stroke volume; SW, stroke work; VAC, ventricular-arterial coupling.

Methods

We conducted a prospective, multicenter observational study of consecutive adults (≥18 years) with CS admitted to four tertiary cardiac centers in Italy and Mexico between July 2023 and October 2024 (see Supplementary File, Methods, and Figure S1, Supplemental Digital Content, https://links.lww.com/ASAIO/B953). Eligibility required Society for Cardiovascular Angiography and Interventions (SCAI) stage ≥B within 24 hours of CS diagnosis. The study was approved by local institutional review boards (INCAR-DG-DI-ACEP-19-2024); written informed consent was obtained, and the study complied with the Declaration of Helsinki (2013) and local regulations.

Hemodynamic Data Acquisition

Pulmonary artery catheter measurements were obtained at baseline and 6, 12, 24, and 48 h. At each time point, right atrial pressure (RAP), pulmonary artery pressures (PAP), pulmonary artery wedge pressure (PAWP), heart rate, arterial-line blood pressure, and cardiac output (CO) by thermodilution were recorded; systemic and pulmonary vascular resistances (SVR, PVR) were derived using standard formulas. Echocardiography was performed within ±30 minutes of PAC sampling to quantify left ventricular ejection fraction (LVEF) by biplane Simpson.[5] Medical treatment was not standardized and varied based on hemodynamic profile, shock phenotype, and local practice. Details regarding vasoactive and inotropic support are provided in Supplementary File and Table S1, Supplemental Digital Content, https://links.lww.com/ASAIO/B953.

Pressure–Volume Loop Surrogate Derivation Formulas

We estimated ventriculo-arterial coupling and energetic indices at the bedside by combining PAC-derived flow with echocardiography-based systolic function to generate indirect PV-plane surrogates using single-beat methods without conductance catheters.

Given the constraints of single-beat estimation in unstable critically ill patients, the volume-axis intercept of the ESPVR (V_0) was assumed to be 0 ml for systolic PV surrogates, consistent with prior single-beat surrogate approaches.[6,7] Thus, absolute (R)Ees values should be interpreted directionally rather than as invasive reference-standard measures. A supplementary sensitivity analysis using V_0 = 20 ml showed consistent directional findings. (see Supplementary File and Tables S2 and S3, Supplemental Digital Content, https://links.lww.com/ASAIO/B953).

In contrast, diastolic properties were parameterized using the Klotz method for the EDPVR,[8,9] using PAWP as a clinical surrogate for LV end-diastolic pressure and EDV as the volume anchor.

- Stroke volume$_{(PAC)}$ = Cardiac output (CO, L/min by thermodilution)/heart rate (bpm)
- End-diastolic volume (EDV) = SV($_{PAC,}$ ml)/LVEF ($_{Echo,}$ 0–1)[10]
- End-systolic volume (ESV) = EDV-SV ($_{PAC}$, ml)[10]

Systolic function derivatives. • End-systolic pressure (ESP, mm Hg) = systolic blood pressure($_{arterial\text{-}line}$, mm Hg) × 0.9[11,12]
- Arterial elastance (Ea, mm Hg/ml) = ESP/SV$_{(PAC)}$[13,14]
- End-systolic LV elastance ((R)Ees, mm Hg/ml) = ESP/(ESV– V_0)[6,7]
- Left ventricular arterial coupling (VAC) = Ea/(R)Ees[7]
- Stroke work (SW, mm Hg·ml) = ESP × SV$_{(PAC)}$[2,15]
- Potential energy (PE, mm Hg·ml) = (ESP × [ESV – V_0])/2[2,15]
- Pressure–volume area (PVA, mm Hg·ml) = SW + PE[2,15]
- Ventricular efficiency (%) = 100 × SW/PVA[6]

Diastolic function. Diastolic function was derived by Klotz et al.[8,9] We measure a single set of EDP [end-diastolic pressure] ≈ PAWP measured and V_m (EDV measured) in ml.

- $\beta = \frac{\text{Log}\left(\frac{P_m}{30}\right)}{\text{Log}\left(\frac{V_m}{V_{30}}\right)}$, and $\alpha = \frac{30}{V_{30}^{\beta}}$

- V_0 = EDV$_m$ (0.6 – 0.006 × PAWP$_m$, mm Hg)[8,9]
- $V_{30} = V_0 + \frac{(V_m - V_0)}{\left(\frac{P_m}{A_n}\right)^{(1/B_n)}}$, where A_n = 27.78 and B_n = 2.76[8,9]

If PAWP was ≤22 mm Hg, then:

If PAWP >22 mm Hg

- $V_{15} = 0.8(V_{30} - V_0) + V_0$
- $\beta = \frac{\text{Log}\left(\frac{P_m}{15}\right)}{\text{Log}\left(\frac{V_m}{V_{15}}\right)}$ and $\alpha = \frac{P_m}{V_{30}^{\beta}}$

A web-based visualization tool was developed (see Supplementary File, Supplemental Digital Content, https://links.lww.com/ASAIO/B953).

Statistical Analyses

Continuous variables are summarized as median (interquartile range [IQR]) and categorical variables as count (%). Baseline between-group comparisons were descriptive and performed using χ^2 or Fisher exact tests for categorical variables and nonparametric tests for continuous variables, as appropriate.

The primary analysis estimated within-patient change from baseline using Bayesian paired models. Each patient contributed one baseline paired assessment (time = 0), and each available follow-up paired assessment at 6, 12, 24, or 48 hours was compared with that baseline, generating "paired snapshots," defined as contemporaneous PAC and echocardiographic measurements obtained within the same clinical window (see Supplementary File and Figure S2, Supplemental Digital Content, https://links.lww.com/ASAIO/B953) When a different tMCS device was introduced, the immediately preceding assessment defined a new baseline, preventing overlap between therapeutic phases. Given variable follow-up, analyses focused on baseline-referenced within-patient change. However, repeated post-baseline change scores from the same patient were modeled using simple Bayesian normal models without patient-level random effects or an explicit longitudinal covariance structure; therefore, residual within-patient dependence may not have been fully accounted for.

Changes from baseline (Δ = after − baseline) were modeled using a Bayesian normal likelihood with weakly informative priors. Posterior sampling was performed using the No-U-Turn Sampler, and convergence was assessed using standard diagnostics. We report the posterior median difference (Δ), the 95% highest density interval (HDI), and $P(\Delta > 0)$. For decreases ($\Delta < 0$), the probability of decrease is interpreted as $1 - P(\Delta > 0)$.

For visualization of relative effect magnitude, symmetric percent change (SPC = 200 × [after − baseline]/[|after| + |baseline|]) was summarized in volcano-style plots; these figures were intended for effect-size representation rather than standalone inferential conclusions. Analyses were conducted in Python 3.11 (PyMC, ArviZ), with additional technical details provided in the Supplementary File, Supplemental Digital Content, https://links.lww.com/ASAIO/B953.

Results

Sixty-eight patients with CS were included; median age was 65 years (IQR, 55.6–73), 75% were male, and 55.9% had AMI-CS. During hospitalization, 33.8% required mechanical ventilation, 20.6% required renal replacement therapy, 33.8% ventricular arrhythmias, and in-hospital mortality was 32.4% (see Supplementary File and Table S4, Supplemental Digital Content, https://links.lww.com/ASAIO/B953). Temporal trends of CSWG-SCAI and tMCS utilization are shown in Figures S3 and S4, Supplemental Digital Content, https://links.lww.com/ASAIO/B953.

Hemodynamic Comparison by the Timing of the tMCS Support

AMI-CS and microaxial flow pump. In AMI-CS + mAFP support (10 patients; 31 paired snapshots), filling pressures and afterload surrogates decreased while forward flow improved (Table 1, Figures 2 and 3; see Table S5, Supplemental Digital Content, https://links.lww.com/ASAIO/B953). Pulmonary artery wedge pressure declined (posterior median Δ − 11.64 mm Hg; 95% HDI, −16.92 to −6.78; probability of decrease 100%), accompanied by reductions in ESP (Δ − 14.38 mm Hg; HDI −21.13 to −7.27; probability of decrease 100%) and Ea (Δ − 1.22 mm Hg /ml; HDI, −1.56 to −0.87; probability of decrease 100%), with improved LV-VAC (Δ − 1.42; HDI, −2.22 to −0.56; probability of decrease 99.9%). Cardiac output increased (Δ + 0.99 L/min; HDI, 0.64–1.43; probability of increase 100%), with a parallel rise in cardiac index (Δ + 0.53 L/min/m^2; HDI, 0.34–0.73; probability of increase 100%). Ventricular efficiency increased (Δ + 6.42%; HDI, 2.73–9.93; probability of increase 100%). Estimated global mechanical energy expenditure showed a probable reduction, as proxy by PVA (Δ − 103.09 mm Hg·ml; HDI, −279.91 to +101.11) and PVA·HR (Δ − 131.39 mm Hg·ml·bpm; HDI, −315.31 to +64.23) probability of decrease of 87.1% and 90.8%, suggesting unloading with a probable trend toward energetic unloading. Right-sided interaction also improved, reflected by a lower RAP/PAWP ratio (Δ − 1.80; HDI, −2.82 to −0.98; probability of decrease 100%) and reduced PVR (Δ − 3.60; HDI, −4.90 to −2.32; probability of decrease 100%). Furthermore, Aortic pulsatility index (API) and Myocardial performance score (MPS) both declined (probability of decrease 97.5% and 97.4%).

HF-CS and microaxial flow pump. In HF-CS + mAFP support (two patients; four paired snapshots), posterior estimates were heterogeneous and limited by wide credible intervals (Table 1, Figures 2 and 3; see Table S6, Supplemental Digital Content, https://links.lww.com/ASAIO/B953). Afterload surrogates showed a reduction in Ea (Δ − 0.35 mm Hg/ml; 95% HDI, −0.61 to −0.10; probability of decrease 98.9%), while perfusion pressure tended to increase (MAP Δ + 7.0 mm Hg; HDI, −2.28 to +16.28; probability of increase 95.2%). Pulmonary pressures demonstrated probable decreases in mPAP (Δ − 3.25 mm Hg; HDI, −6.78 to +0.28; probability of decrease 97.0%) and PAWP (Δ − 4.50 mm Hg; HDI, −10.09 to +1.09; probability of decrease 95.8%). The PV-derived energetic indices did not show consistent evidence of unloading (PVA Δ + 1,323.86 mm Hg·ml; HDI, −3,271.68 to +5,919.40), whereas diastolic parameters exhibited shifts consistent with improved compliance ($\alpha\ \Delta$ − 1.53×10^{-5}; HDI -3.14×10^{-5} to $+7.91 \times 10^{-7}$; probability of decrease 97.2%; $\beta\ \Delta$ + 0.48; HDI −0.05 to +1.01; probability of increase 96.8%). The MPS demonstrated a weak positive effect (probability of increasing 73.4%). Given the small sample size, these findings should be interpreted as exploratory.

AMI-CS supported with IABP. In AMI-CS + IABP (20 patients; 70 paired snapshots), pulmonary and left-sided filling pressures declined (Table 1, Figures 2 and 3; see Table S7, Supplemental Digital Content, https://links.lww.com/ASAIO/B953). Pulmonary artery wedge pressure decreased by Δ − 10.42 mm Hg (95% HDI, −12.61 to −8.16; probability of decrease 100%), accompanied by reductions in pulmonary artery pressures (*e.g.*, mPAP Δ − 5.03 mm Hg; HDI, −7.26 to −2.62; probability of decrease 100%), while MAP remained unchanged (Δ − 0.09 mm Hg; HDI, −3.74 to +3.34). Forward flow showed only modest changes (CO Δ + 0.20 L/min; HDI, −0.05 to +0.44; probability of increase 94.6%), whereas perfusion surrogates improved, including a rise in organ perfusion

Table 1. Bayesian HDI With 95% CIs and Likelihood P(Δ > 0) of Hemodynamic and Ventricular Changes Across Cardiogenic Shock Etiologies and Support Strategies

	AMI-CS mAFP, HDI	P (Δ > 0)	HF-CS mAFP, HDI	P(Δ > 0)
Baseline Patients/Paired Snapshots	(n = 10/31)		(n = 2/4)	
Heart rate (bpm)	2.03 (–4.47 to 8.83)	0.744	–11.00 (–28.53 to 6.53)	0.07
SBP (mm Hg)	–16.23 (–23.74 to –8.08)	0	4.25 (–17.23 to 25.73)	0.713
DBP (mm Hg)	–8.80 (–13.94 to –3.47)	0.001	8.50 (–0.64 to 17.64)	0.97
MAP (mm Hg)	–13.02 (–18.25 to –7.55)	0	7.00 (–2.28 to 16.28)	0.952
sPAP (mm Hg)	–7.00 (–11.55 to –2.64)	0.003	–3.00 (–8.66 to 2.66)	0.095
dPAP (mm Hg)	–5.54 (–9.82 to –1.11)	0.006	–3.00 (–7.68 to 1.68)	0.067
mPAP (mm Hg)	–6.28 (–10.35 to –2.27)	0.003	–3.25 (–6.78 to 0.28)	0.03
PAWP (mm Hg)	–11.64 (–16.92 to –6.78)	0	–4.50 (–10.09 to 1.09)	0.042
RAP (mm Hg)	1.65 (–1.53 to 4.52)	0.864	–2.75 (–10.80 to 5.30)	0.178
Cardiac output (L/min)	0.99 (0.64–1.43)	1	0.32 (–0.55 to 1.19)	0.836
pH	0.06 (0.03–0.09)	1	0.00 (–0.08 to 0.07)	0.46
HCO3 (mEq/L)	0.78 (–0.95 to 2.44)	0.822	2.73 (–2.45 to 7.90)	0.904
Lactate (mmol/L)	–0.02 (–1.11 to 0.98)	0.491	–1.69 (–7.61 to 4.24)	0.216
$SvcO_2$ (%)	4.06 (0.23–7.57)	0.979	ND	ND
Left ventricular function–derived variables				
SV (ml)	9.02 (4.89–12.78)	1	8.52 (–4.18 to 21.22)	0.939
SVi (ml)	4.84 (2.87–6.83)	1	3.79 (–1.56 to 9.14)	0.945
Cardiac index (L/min/m^2)	0.53 (0.34–0.73)	1	0.15 (–0.22 to 0.52)	0.856
SVR (dynes·sec·cm^{-5})	–243.95 (–388.63 to –103.44)	0.002	81.87 (–227.30 to 391.04)	0.769
SVRi (dynes·sec·cm^{-5})	–288.97 (–455.79 to –106.49)	0.002	185.62 (–513.16 to 884.40)	0.77
LVSWi (g·m/m^2)	0.90 (–1.26 to 2.83)	0.807	6.30 (–3.23 to 15.83)	0.937
CPO (W)	0.089 (0.023–0.144)	0.998	0.137 (–0.121 to 0.394)	0.905
CPI (W/m^2)	0.047 (0.016–0.078)	0.998	0.061 (–0.048 to 0.171)	0.914
CPI–RAP (W/m^2)	0.08 (0.04–0.119)	1	0.078 (–0.026 to 0.182)	0.951
API	–7.83 (–15.4 to 0.37)	0.025	0.19 (–2.99 to 3.34)	0.619
MPS	–2.35 (–4.83 to 0.039)	0.026	0.32 (–2.01 to 1.84)	0.734
Right ventricular function–derived variables				
RAP/PAWP	–1.80 (–2.82 to –0.98)	0	–0.08 (–0.34 to 0.18)	0.2
PAPI	2.10 (0.47–3.89)	0.99	0.21 (–0.04 to 0.46)	0.963
PVR (dynes·sec·cm^{-5})	–3.60 (–4.90 to –2.32)	0	–0.44 (–2.75 to 1.87)	0.293
PVRi (dynes·sec·cm^{-5})	–6.61 (–9.15 to –4.30)	0.001	–0.95 (–6.04 to 4.14)	0.297
Pulmonary artery compliance (ml/mm Hg)	0.86 (0.43–1.25)	1	0.63 (–0.45 to 1.71)	0.92
RVSWi (g·m/m^2)	2.54 (1.69–3.43)	1	0.91 (–0.73 to 2.55)	0.913
Perfusion pressure variables				
OPP (mm Hg)	–1.29 (–8.90 to 6.12)	0.369	11.50 (–0.72 to 23.72)	0.971
CPP (mm Hg)	–10.26 (–14.62 to –5.50)	0	11.25 (–4.73 to 27.23)	0.945
Echocardiographic variables				
LVEF (%)	4.58 (2.03–7.20)	0.999	3.75 (–8.18 to 15.68)	0.804
Tricuspid S´(cm/s)	2.43 (0.92–3.87)	0.998	1.67 (–5.50 to 8.84)	0.789
TAPSE (mm)	2.03 (0.37–3.65)	0.989	0.33 (–1.10 to 1.77)	0.789
VAC RV (TAPSE/sPAP, mm/mm Hg)	0.16 (0.08–0.23)	0.999	0.07 (–0.23 to 0.37)	0.789
PV loops				
End-diastolic volume (ml)	–2.94 (–38.21 to 29.69)	0.429	7.52 (–93.15 to 108.18)	0.586
End-systolic volume (ml)	–11.26 (–42.57 to 20.52)	0.238	–1.00 (–107.73 to 105.72)	0.489
End-systolic pressure (mm Hg)	–14.38 (–21.13 to –7.27)	0	3.82 (–15.51 to 23.16)	0.713
Arterial elastance (mm Hg/ml)	–1.22 (–1.56 to –0.87)	0	–0.35 (–0.61 to –0.10)	0.011
End-systolic LV elastance ((R)Ees mm Hg/ml)	–0.12 (–0.32 to 0.07)	0.102	0.07 (–0.35 to 0.50)	0.694
LV-VAC	–1.42 (–2.22 to –0.56)	0.001	–0.82 (–3.49 to 1.85)	0.2
SW (mm Hg·ml)	140.32 (–32.82 to 301.55)	0.951	1,178.45 (–1,241.65 to 3,598.56)	0.891
PE (mm Hg·ml)	–167.65 (–345.22 to 15.15)	0.028	145.41 (–4,949.79 to 5,240.60)	0.533
PVA (mm Hg·ml)	–103.09 (–279.91 to 101.11)	0.129	1,323.86 (–3,271.68 to 5,919.40)	0.787
PVA × HR (mm Hg·ml·bpm)	–131.39 (–315.31 to 64.23)	0.092	–78,356.25 (–605,320.97 to 448,608.47)	0.334
Ventricular efficiency (%)	6.42 (2.73–9.93)	1	5.02 (–10.95 to 20.98)	0.804
α	4.41 (0.49–8.12)	0.991	–1.53E-05 (–3.14E-05 to 7.91E-07)	0.028
β	–0.36 (–0.82 to 0.04)	0.048	0.48 (–0.05 to 1.01)	0.968
V_0 (ml)	–4.18 (–27.40 to 15.91)	0.363	7.66 (–34.39 to 49.70)	0.699
V_{30} (ml)	–33.69 (–94.63 to 32.03)	0.151	14.47 (–80.23 to 109.17)	0.67
Other variables				
LVIS	3.02 (–2.97 to 8.27)	0.86	3.50 (–9.78 to 16.78)	0.768

α, EDPVR slope (alpha constant); β, EDPVR curvature (beta constant); API, aortic pulsatility index; CI, confidence interval; CO, cardiac output; CPI, cardiac power index; CPI-RAP, CPI adjusted for RAP; CPO, cardiac power output; CPP, coronary perfusion pressure; DBP, diastolic blood pressure; dPAP, diastolic pulmonary artery pressure; Ea, arterial elastance; ESP, end-systolic pressure; Hb, hemoglobin; HCO_3^-, bicarbonate; HDI, highest density interval; HR, heart rate; LVEF, left ventricular ejection fraction; LVIS, Levosimendan vasoactive inotropic score; LVSW, left ventricular stroke work; LVSWi, left ventricular stroke work index; MAP, mean arterial pressure; mPAP, mean pulmonary artery pressure; MPS, Myocardial Performance Score; OPP, organ perfusion pressure; PAPI, pulmonary artery pulsatility index; PAWP, pulmonary artery wedge pressure; PE, potential energy; pH, arterial pH; PVA, pressure–volume área; PVR, pulmonary vascular resistance; PVRi, pulmonary vascular resistance index; (R)Ees, end-systolic LV elastance; RAP, right atrial pressure; RAP/PAWP, RAP to PAWP ratio; RVSW, right ventricular stroke work; RVSWi, right ventricular stroke work index; SBP, systolic blood pressure; sPAP, systolic pulmonary artery pressure; SV, stroke volume; SVi, stroke volume index; SvO_2, central venous oxygen saturation; SVR, systemic vascular resistance; SVRi, systemic vascular resistance index; SW, stroke work; TAPSE, tricuspid annular plane systolic excursión; V_0, volume-axis intercept; V_{30}, volume at end-diastolic pressure of 30 mm Hg; VAC, ventricular arterial coupling.

AMI-CS IABP, HDI	P (Δ > 0)	HF-CS IABP, HDI	P (Δ > 0)	AMI-CS No MCS, HDI	P (Δ > 0)	HF-CS No MCS, HDI	P (Δ > 0)
(n = 20/70)		(n = 7/12)		(n = 8/25)		(n = 22/52)	
3.06 (−0.54 to 6.72)	0.951	−12.37 (−22.58 to −2.83)	0.008	−3.81 (−9.96 to 2.23)	0.105	3.71 (−1.22 to 8.32)	0.937
1.91 (−2.43 to 6.28)	0.808	26.73 (8.94–43.74)	0.999	−11.49 (−20.80 to −1.89)	0.009	−0.80 (−5.19 to 2.88)	0.352
−1.90 (−5.82 to 1.47)	0.158	−1.39 (−9.67 to 7.02)	0.346	−6.50 (−10.70 to −2.55)	0.002	−1.16 (−4.24 to 1.74)	0.222
−0.09 (−3.74 to 3.34)	0.5	14.25 (3.36–24.11)	0.996	−7.41 (−12.04 to −2.16)	0.004	−0.35 (−3.30 to 2.85)	0.398
−6.06 (−9.25 to −3.02)	0.001	−5.91 (−14.09 to 0.88)	0.045	−3.37 (−8.14 to 2.00)	0.087	−4.00 (−8.01 to −0.44)	0.02
−4.74 (−7.00 to −2.56)	0	−3.67 (−7.57 to 0.20)	0.027	−1.71 (−4.93 to 2.26)	0.161	−5.57 (−7.83 to −3.20)	0
−5.03 (−7.26 to −2.62)	0	−4.42 (−9.31 to 0.53)	0.04	−2.04 (−5.90 to 1.94)	0.146	−5.20 (−7.99 to −2.46)	0
−10.42 (−12.61 to −8.16)	0	−4.68 (−8.43 to −1.17)	0.004	−5.49 (−7.21 to −3.77)	0	−9.13 (−11.81 to −6.65)	0
1.71 (−0.13 to 3.61)	0.964	−8.31 (−12.94 to −3.73)	0.001	1.18 (−3.44 to 5.69)	0.712	−1.37 (−3.81 to 1.01)	0.12
0.20 (−0.05 to 0.44)	0.946	0.28 (−0.45 to 1.01)	0.8	0.40 (−0.16 to 0.95)	0.927	0.77 (0.47–1.08)	1
0.06 (0.04–0.08)	1	0.11 (0.02–0.22)	0.983	0.13 (0.07–0.20)	1	0.03 (−0.01 to 0.06)	0.935
4.44 (3.63–5.35)	1	8.88 (4.13–14.16)	0.998	3.88 (1.70–6.40)	0.998	2.75 (1.07–4.61)	0.999
−1.46 (−1.92 to −1.00)	0	−3.80 (−7.63 to −0.10)	0.027	−1.36 (−1.98 to −0.77)	0	−0.24 (−0.65 to 0.13)	0.108
3.37 (0.51–5.77)	0.994	ND	ND	−2.78 (−6.46 to 0.78)	0.054	6.46 (0.74–12.67)	0.977
1.69 (−0.98 to 4.32)	0.904	7.35 (−0.68 to 16.49)	0.958	4.65 (−0.13 to 9.89)	0.966	6.59 (2.53–11.06)	0.997
0.80 (−0.66 to 2.37)	0.867	4.11 (−0.12 to 8.53)	0.968	2.24 (−0.62 to 5.11)	0.947	3.91 (1.78–6.33)	0.999
0.09 (−0.03 to 0.24)	0.897	0.16 (−0.25 to 0.51)	0.831	0.19 (−0.10 to 0.45)	0.921	0.44 (0.28–0.58)	1
103.75 (7.53–198.60)	0.98	120.34 (−37.74 to 269.08)	0.939	−174.51 (−341.59 to −4.52)	0.02	−78.05 (−191.01 to 33.72)	0.092
141.72 (12.03–270.71)	0.974	126.86 (−37.03 to 300.45)	0.937	−188.05 (−377.84 to −12.56)	0.024	−146.91 (−293.39 to −12.23)	0.019
−0.42 (−2.40 to 1.38)	0.324	9.67 (5.61–13.66)	1	0.942 (−2.356 to 4.255)	0.727	3.86 (1.73–5.96)	1
0.025 (−0.036 to 0.077)	0.816	0.16 (0.02–0.31)	0.985	0.017 (−0.102 to 0.14)	0.603	0.139 (0.083–0.192)	1
0.012 (−0.021 to 0.043)	0.777	0.088 (0.013–0.168)	0.978	0.001 (−0.07 to 0.062)	0.513	0.08 (0.05–0.106)	1
0.05 (0.02–0.079)	1	0.1 (0.034–0.161)	0.992	0.028 (−0.035 to 0.087)	0.832	0.105 (0.076–0.135)	1
−0.42 (−1.09 to 0.2)	0.096	4.94 (1.68–7.92)	0.995	−0.93 (−2.87 to 1.21)	0.174	0.29 (−0.27 to 0.86)	0.841
−0.12 (−0.34 to 0.14)	0.156	1.71 (0.84–2.64)	1	0.07 (−0.53 to 0.76)	0.592	0.33 (0.07–0.58)	0.992
−1.10 (−1.31 to −0.87)	0	0.036 (−0.11 to 0.192)	0.693	−0.78 (−1.11 to −0.43)	0	−0.60 (−0.82 to −0.41)	0
1.27 (0.75–1.87)	1	0.83 (0.17–1.58)	0.984	0.86 (0.26–1.47)	0.996	3.77 (2.45–5.29)	1
−2.46 (−3.34 to −1.60)	0	0.59 (−0.59 to 1.77)	0.862	−1.39 (−2.56 to −0.39)	0.007	−2.62 (−3.66 to −1.56)	0
−4.69 (−6.35 to −2.95)	0	1.09 (−1.06 to 3.36)	0.857	−2.68 (−4.88 to −0.42)	0.01	−4.75 (−6.53 to −3.01)	0
0.25 (−0.10 to 0.62)	0.917	0.47 (−0.17 to 1.11)	0.937	1.06 (0.03–2.10)	0.975	0.25 (−0.04 to 0.49)	0.961
1.89 (1.34–2.54)	1	1.10 (−0.54 to 2.60)	0.913	0.76 (−0.28 to 1.81)	0.927	2.37 (1.33–3.47)	1
10.31 (6.40–14.61)	1	18.74 (9.45–28.01)	1	−2.07 (−6.91 to 4.16)	0.221	9.50 (5.28–13.24)	1
−3.54 (−8.21 to 0.70)	0.053	6.65 (−0.47 to 13.42)	0.965	−7.77 (−14.41 to −2.29)	0.006	0.24 (−2.50 to 3.36)	0.561
3.06 (1.34–4.67)	1	1.68 (−0.09 to 3.68)	0.959	2.06 (−0.66 to 5.08)	0.929	1.78 (0.35–3.07)	0.993
0.00 (−1.19 to 1.16)	0.499	−0.10 (−0.49 to 0.28)	0.286	1.93 (0.38–3.47)	0.992	1.66 (0.81–2.54)	1
1.00 (0.29–1.71)	0.994	0.33 (−0.08 to 0.74)	0.943	0.02 (−0.69 to 0.67)	0.519	0.34 (−0.09 to 0.78)	0.944
0.08 (0.03–0.12)	0.999	0.06 (−0.01 to 0.12)	0.963	0.11 (0.05–0.18)	0.998	0.08 (0.04–0.12)	1
−10.23 (−23.18 to 4.33)	0.058	40.93 (−14.68 to 94.23)	0.934	15.23 (−14.56 to 42.05)	0.868	23.95 (0.64–50.67)	0.971
−11.86 (−23.79 to 0.12)	0.029	33.97 (−21.70 to 85.32)	0.911	10.47 (−13.29 to 35.01)	0.812	18.14 (−2.25 to 39.28)	0.949
1.82 (−1.83 to 5.61)	0.828	23.89 (6.66–38.96)	0.995	−10.43 (−18.31 to −1.42)	0.007	−0.74 (−4.46 to 2.74)	0.332
−0.07 (−0.29 to 0.13)	0.24	−0.17 (−0.83 to 0.54)	0.303	−1.41 (−2.46 to −0.30)	0.005	−0.49 (−0.80 to −0.18)	0.003
0.13 (0.01–0.26)	0.979	0.06 (−0.09 to 0.20)	0.816	−0.26 (−0.62 to 0.13)	0.085	0.01 (−0.12 to 0.14)	0.576
−0.42 (−0.72 to −0.15)	0.003	−0.49 (−1.25 to 0.19)	0.069	−0.07 (−0.40 to 0.24)	0.333	−0.32 (−0.56 to −0.04)	0.009
85.73 (−60.26 to 232.91)	0.876	249.61 (57.28–425.92)	0.996	23.21 (−144.41 to 175.94)	0.61	225.94 (53.08–380.56)	0.995
−111.10 (−283.85 to 54.03)	0.096	201.65 (13.00–405.04)	0.982	5.13 (−176.92 to 167.32)	0.536	155.29 (−11.60 to 356.56)	0.959
−45.58 (−229.30 to 116.95)	0.31	220.59 (22.39–408.81)	0.983	15.34 (−175.27 to 209.79)	0.559	196.44 (7.60–370.84)	0.983
−50.61 (−233.66 to 141.03)	0.282	190.22 (7.21–384.64)	0.975	10.39 (−186.75 to 196.61)	0.54	307.60 (100.06–502.61)	0.999
3.58 (1.66–5.56)	1	2.41 (−0.69 to 5.43)	0.94	1.91 (−1.16 to 5.09)	0.895	2.20 (0.44–3.75)	0.993
3.12 (1.02–5.34)	0.996	−7.1E-06 (−1.52E-05 to 1.4E-06)	0.036	4.10 (0.18–8.42)	0.971	4.98 (2.21–7.91)	0.997
−0.28 (−0.52 to −0.05)	0.011	0.01 (−0.21 to 0.24)	0.539	−0.38 (−0.82 to 0.10)	0.056	−0.48 (−0.85 to −0.11)	0.005
−6.94 (−14.42 to 0.14)	0.031	33.76 (2.54–65.61)	0.98	8.51 (−5.85 to 22.28)	0.889	13.90 (−1.03 to 27.45)	0.971
−17.17 (−36.18 to −2.70)	0.022	66.74 (3.49–130.87)	0.977	18.90 (−12.06 to 49.33)	0.897	29.55 (−2.60 to 56.09)	0.973
−9.25 (−16.27 to −1.71)	0.007	−5.86 (−12.61 to 0.57)	0.038	−3.36 (−7.60 to 1.19)	0.056	1.23 (−1.99 to 4.61)	0.78

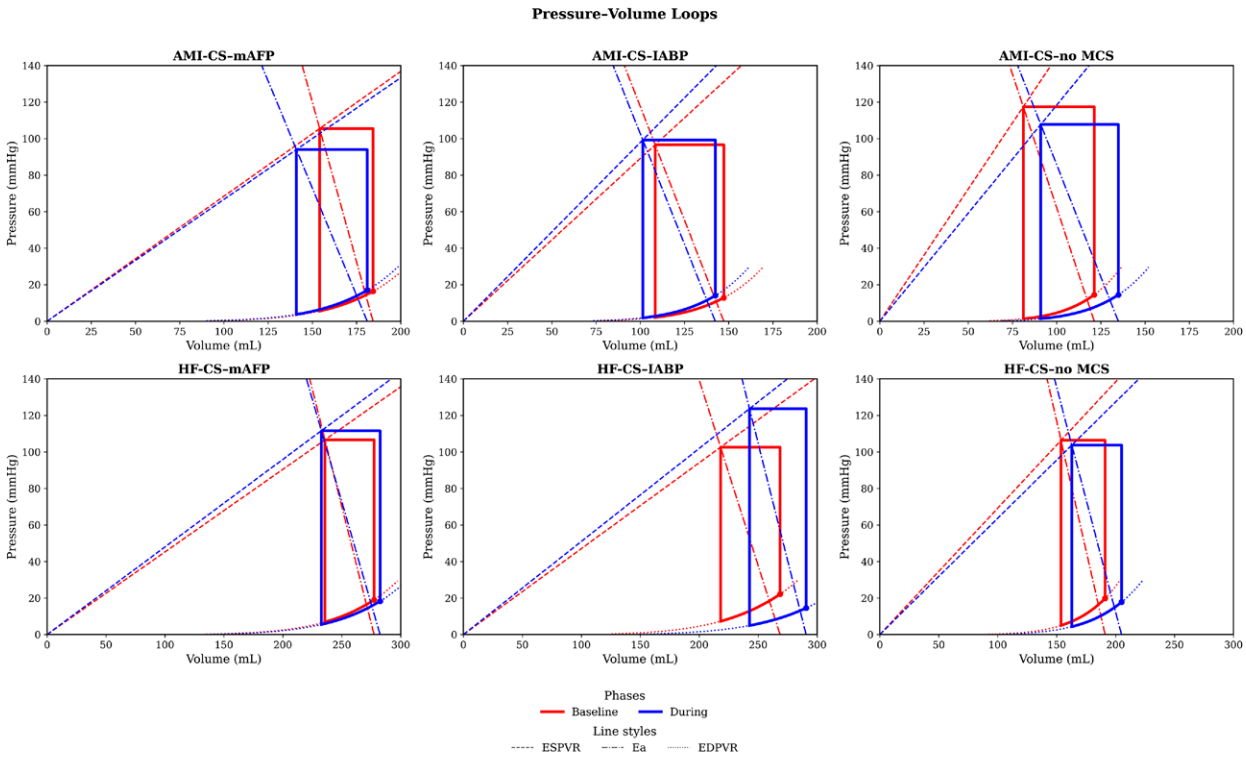

Figure 2. Dynamics of PV-loop surrogates across cardiogenic shock phenotypes and mechanical support strategies. Representative PV loops surrogates at baseline (red) and during support (blue) in patients with cardiogenic shock due to AMI (top panels) or decompensated HF (bottom panels), stratified by device type: mAFP, IABP, and no mechanical circulatory support (no tMCS). All PV-loops surrogates were generated from group-level mean values at each time point. AMI, acute myocardial infarction; HF, heart failure; IABP, intra-aortic balloon pump; mAFP, microaxial flow pump; PV, pressure–volume; tMCS, temporary mechanical circulatory support.

pressure (OPP, Δ + 10.31 mm Hg; HDI, 6.40–14.61; probability of increase 100%) and SvO_2 (Δ + 3.37%; HDI, 0.51–5.77; probability of increase 99.4%). Right-sided interaction improved, reflected by a marked reduction in RAP/PAWP (Δ − 1.10; HDI, −1.31 to −0.87; probability of decrease 100%), increased PAPI (Δ + 1.27; HDI, 0.75–1.87; probability of increase 100%), and reduced PVR (Δ − 2.46 dyn·s·cm^{-5}; HDI, −3.34 to −1.60; probability of decrease 100%). The PV-derived systolic coupling showed a modest improvement (LV-VAC Δ − 0.42; HDI, −0.72 to −0.15; probability of decrease 99.7%) with increased ventricular efficiency (Δ + 3.58%; HDI, 1.66–5.56; probability of increase 100%), while energetic demand indices (PVA and PVA·HR) did not demonstrate a consistent reduction; and diastolic parameters derived from the Klotz method evolved in a direction consistent with improved compliance.

HF-CS supported with IABP. In HF-CS + IABP (seven patients; 12 paired snapshots), systemic augmentation and decongestion occurred in parallel (Table 1, Figures 2 and 3; see Table S8, Supplemental Digital Content, https://links.lww.com/ASAIO/B953). Systolic pressure and MAP increased (SBP Δ + 26.73 mm Hg; 95% HDI, 8.94–43.74; probability of increase 99.9%; MAP Δ + 14.25 mm Hg; HDI, 3.36–24.11; probability of increase 99.6%), while filling pressures declined (PAWP Δ − 4.68 mm Hg; HDI, −8.43 to −1.17; probability of decrease 99.6%) with a concurrent reduction in RAP (Δ − 8.31 mm Hg; HDI, −12.94 to −3.73; probability of decrease 99.9%). Cardiac output changes were modest and uncertain (Δ + 0.28 L/min; HDI, −0.45 to +1.01), whereas perfusion surrogates improved, including higher OPP (Δ + 18.74 mm Hg; HDI, 9.45–28.01; probability of increase 100%) and increased cardiac power indexed to RAP (CPI-RAP Δ + 0.10 W/m^2; HDI, 0.034–0.161; probability of increase 99.2%).

Pressure–volume–derived systolic loading reflected augmentation rather than unloading, with increased ESP (Δ + 23.89 mm Hg; HDI, 6.66–38.96; probability of increase 99.5%) and larger volumes (EDV Δ + 40.93 ml; HDI, −14.68 to +94.23; probability of increase 93.4%). Estimated energetic indices increased, with higher stroke work (Δ + 249.61 mm Hg·ml; HDI, 57.28–425.92; probability of increase 99.6%) and PVA (Δ + 220.59 mm Hg·ml; HDI, 22.39–408.81; probability of increase 98.3%), suggesting improved mechanical output at the expense of higher estimated energetic demand. Diastolic parameters showed a probable shift consistent with improved compliance (α Δ − 7.1 × 10^{-6}; HDI −1.52 × 10^{-5} to +1.4 × 10^{-6}; probability of decrease 96.4%), while β remained unchanged; both API (Δ4.94; HDI, 1.68–7.92; probability of increase 99.5%) and MPS (Δ1.71; HDI 0.84–2.64; probability of increase 100%) increased.

AMI-CS without tMCS. In AMI-CS managed medically (eight patients; 25 paired snapshots; Table 1, Figures 2 and 3; see Table S9, Supplemental Digital Content, https://links.lww.com/ASAIO/B953), systemic pressures declined (SBP

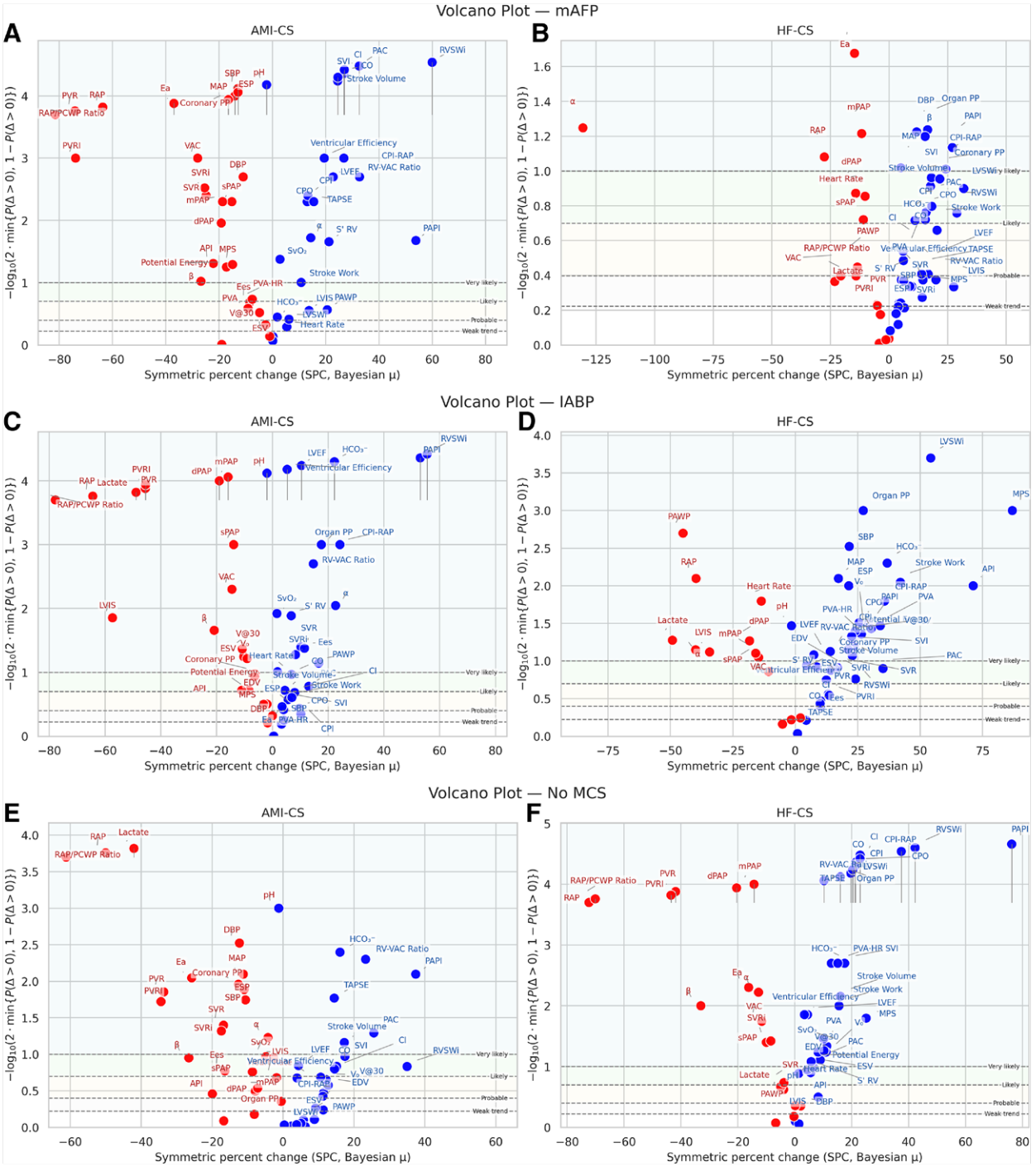

Figure 3. Bayesian volcano plots of hemodynamic response to mechanical circulatory support (tMCS). Volcano plots summarize the magnitude and posterior certainty of change in hemodynamic, metabolic, and ventricular-mechanics variables after tMCS initiation across etiological phenotypes of cardiogenic shock. The x-axis represents the SPC (Bayesian μ) relative to baseline, and the y-axis shows posterior certainty [$-\log_{10}(2 \times \min\{P(\Delta > 0), 1 - P(\Delta > 0)\})$]. Red markers denote decreases and blue markers denote increases compared with baseline. Dashed horizontal lines indicate probabilistic evidence thresholds (weak trend, probable, likely, very likely). **A–B**: mAFP. **C–D**: IABP. **E–F**: no tMCS. IABP, intra-aortic balloon pump; mAFP, microaxial flow pump; SPC, symmetric percent change.

Δ − 11.49 mm Hg; 95% HDI, −20.80 to −1.89; probability of decrease 99.1%; MAP Δ − 7.41 mm Hg; HDI, −12.04 to −2.16; probability of decrease 99.6%) alongside a reduction in left-sided filling pressure (PAWP Δ − 5.49 mm Hg; HDI, −7.21 to −3.77; probability of decrease 100%). Afterload surrogates also decreased, including ESP (Δ − 10.43 mm Hg; HDI, −18.31

to −1.42; probability of decrease 99.3%) and Ea (Δ − 1.41 mm Hg/ml; HDI, −2.46 to −0.30; probability of decrease 99.5%), with concomitant reductions in SVR/SVRi. Forward flow changes were modest and uncertain (CO Δ + 0.40 L/min; HDI, −0.16 to +0.95). Right-sided interaction improved despite no device support, with a lower RAP/PAWP ratio (Δ − 0.78; HDI, −1.11 to −0.43; probability of decrease 100%), higher PAPI (Δ + 0.86; HDI +0.26 to +1.47; probability of increase 99.6%), reduced PVR (Δ − 1.39; HDI, −2.56 to −0.39; probability of decrease 99.3%), and increased pulmonary artery compliance (Δ + 1.06 ml/mm Hg; HDI, 0.03–2.10; probability of increase 97.5%). Pressure-volume–derived energetic indices (SW, PVA, and PVA·HR) did not demonstrate consistent changes.

HF-CS without tMCS. In HF-CS managed medically (22 patients; 52 paired snapshots), pulmonary and left-sided filling pressures declined (Table 1, Figures 2 and 3; see Table S10, Supplemental Digital Content, https://links.lww.com/ASAIO/B953). Pulmonary artery wedge pressure decreased (Δ − 9.13 mm Hg; 95% HDI, −11.81 to −6.65; probability of decrease 100%) alongside reductions in pulmonary artery pressures (mPAP Δ − 5.20 mm Hg; HDI, −7.99 to −2.46; probability of decrease 100%), while systemic pressures remained unchanged (MAP Δ − 0.35 mm Hg; HDI, −3.30 to +2.85). Forward flow and perfusion surrogates improved despite no device support, with increases in cardiac output (Δ + 0.77 L/min; HDI, 0.47–1.08; probability of increase 100%), cardiac index (Δ + 0.44 L/min/m^2; HDI, 0.28–0.58; probability of increase 100%), and CPI-RAP (Δ + 0.105 W/m^2; HDI, 0.076–0.135; probability of increase 100%), together with higher OPP (Δ + 9.50 mm Hg; HDI, 5.28–13.24; probability of increase 100%). Right-sided interaction improved substantially, with a lower RAP/PAWP ratio (Δ − 0.60; HDI, −0.82 to −0.41; probability of decrease 100%), higher PAPI (Δ + 3.77; HDI, 2.45–5.29; probability of increase 100%), and reduced PVR (Δ − 2.62; HDI, −3.66 to −1.56; probability of decrease 100%). Pressure–volume–derived afterload surrogates also decreased (Ea Δ − 0.49 mm Hg/ml; HDI, −0.80 to −0.18; probability of decrease 99.7%), with a modest improvement in LV-VAC (Δ − 0.32; HDI, −0.56 to −0.04; probability of decrease 99.1%). Whereas energetic indices increased (SW Δ + 225.94 mm Hg·ml; HDI, 53.08–380.56; probability of increase 99.5%; PVA Δ + 196.44 mm Hg·ml; HDI, 7.60–370.84; probability of increase 98.3%; PVA·HR Δ + 307.60 mm Hg·ml·bpm; HDI, 100.06–502.61; probability of increase 99.9%), indicating improved mechanical output with higher estimated energetic demand. API showed a probable increase, whereas MPS showed a very likely increase.

Integrated response patterns. Pressure–volume–loop surrogates showed different patterns across devices and shock types. In AMI-CS, mAFP indicated pressure unloading and improved efficiency, while IABP primarily aided decongestion and right-sided coupling without reducing overall energy use. In HF-CS, exploratory subgroup analyses suggested a tendency toward increased mechanical output and cardiac power with IABP or medical therapy. Posterior probabilities were sorted into likelihood tiers, visualizing device- and phenotype-specific change patterns (Table 2). These descriptive findings suggest that device effects may vary by shock phenotype and that PV-surrogate indices may complement bedside interpretation beyond pressure and flow metrics, although confirmation in larger cohorts is required (Figure 3).

Discussion

This multicenter CS cohort shows that estimating bedside indirect single-beat PV-loop surrogates from pulmonary artery catheter and echocardiography is feasible. Pressure–volume–derived surrogates suggest device- and etiology-specific coupling and energetic patterns not always captured by pressure–flow variables (Visual abstract).

Derivation of Bedside Pressure–Volume–Loop Surrogates Using Integrated Pulmonary Artery Catheter and Echocardiography

In critically ill patients on tMCS, noninvasive echocardiography may be limited, especially for estimating left-sided pressures; combining PAC measurements with echocardiographic systolic function offers robust inputs for bedside PV-loop surrogates estimation.[16,17] Left ventricular volumes were estimated from SV and LVEF (EDV from SV/LVEF; ESV = EDV − SV),[10] and coupling was summarized using Ea/(R)Ees under conventional single-beat assumptions.[7,18,19] Because these metrics are derived indirectly and rely on modeling assumptions (including ESP estimation and volume-axis intercepts), they should be interpreted as contextual surrogates for tracking physiological trajectories rather than as direct replacements for invasive PV measurements. This pragmatic integration may be useful when transport is impractical and serial invasive PV acquisition is not feasible. An interactive web-based visualization tool was developed to facilitate bedside interpretation of PV-derived indices and trajectory tracking (see Supplementary File, Supplemental Digital Content, https://links.lww.com/ASAIO/B953).

The assumption of V_0 = 0 is more acceptable in AMI-CS, where ventricular geometry is less altered, compared with HF-CS, where remodeling and dilation make a non-negligible unstressed volume less plausible. Sensitivity analyses with V_0 = 20 ml showed consistent overall results, although some comparisons crossed interpretive thresholds. These shifts indicate V_0 mainly affected support strength, not the qualitative effect's direction. Overall, supporting the robustness of physiological interpretations, but HF phenotypes may be more sensitive to this assumption (see Supplementary File and Tables S2 and S3, Supplemental Digital Content, https://links.lww.com/ASAIO/B953).

Impact of tMCS on Hemodynamics and Pressure–Volume Loops

In AMI-CS, mAFP support was associated with a PV-surrogate pattern that suggested unloading and improved ventriculo-arterial coupling, including lower ESP and reduced Ea. Posterior probabilities favored lower PVA and PVA·HR, and an increased mechanical efficiency,[20] and reduced Ea led to improved VAC.[20–23] Left ventricular efficiency peaked during mAFP, consistent with hemodynamic unloading that could enhance collateral flow and myocardial recovery.[20,24] Unlike other tMCS, EDV/ESV did not increase, likely due to lower PAWP, improved MAP, and reduced LV wall stress.[20,21] Estimates indicate significant reductions in filling pressures and afterload, with improvements in flow, power, and biventricular interaction. Right-sided measures also improved, with lower RAP/PAWP and PVR and higher PAPI, indicating

Table 2. Directional Summary of Bayesian Posterior Changes Across Support Strategies

Variable	AMI-CS mAFP	HF-CS mAFP	AMI-CS IABP	HF-CS IABP	AMI-CS No MCS	HF-CS No MCS
Heart rate (bpm)	↗	↓↓	↑↑↑	↓↓↓	↓	↑↑
SBP (mm Hg)	↓↓↓	↗	↑	↑↑↑	↓↓↓	↔
DBP (mm Hg)	↓↓↓	↑↑↑	↓	↔	↓↓↓	↘
MAP (mm Hg)	↓↓↓	↑↑↑	↔	↑↑↑	↓↓↓	↔
sPAP (mm Hg)	↓↓↓	↓↓	↓↓↓	↓↓↓	↓↓	↓↓↓
dPAP (mm Hg)	↓↓↓	↓↓	↓↓↓	↓↓↓	↓	↓↓↓
mPAP (mm Hg)	↓↓↓	↓↓↓	↓↓↓	↓↓↓	↓	↓↓↓
PAWP (mm Hg)	↓↓↓	↓↓↓	↓↓↓	↓↓↓	↓↓↓	↓↓↓
RAP (mm Hg)	↑	↓	↑↑↑	↓↓↓	↗	↓
Cardiac output (L/min)	↑↑↑	↑	↑↑	↑	↑↑	↑↑↑
pH	↑↑↑	↔	↑↑↑	↑↑↑	↑↑↑	↑↑
HCO3 (mEq/L)	↑	↑↑	↑↑↑	↑↑↑	↑↑↑	↑↑↑
Lactate (mmol/L)	↔	↘	↓↓↓	↓↓↓	↓↓↓	↓
$SvcO_2$ (%)	↑↑↑	—	↑↑↑	—	↓↓	↑↑↑
Left ventricular function–derived variables						
SV (ml)	↑↑↑	↑↑	↑↑	↑↑↑	↑↑↑	↑↑↑
SVi (ml)	↑↑↑	↑↑	↑	↑↑↑	↑↑	↑↑↑
Cardiac index (L/min/m^2)	↑↑↑	↑	↑	↑	↑↑	↑↑↑
SVR (dynes·sec·cm^{-5})	↓↓↓	↗	↑↑↑	↑↑	↓↓↓	↓↓
SVRi (dynes·sec·cm^{-5})	↓↓↓	↗	↑↑↑	↑↑	↓↓↓	↓↓↓
LVSWi (g·m/m^2)	↑	↑↑	↔	↑↑↑	↗	↑↑↑
CPO (W)	↑↑↑	↑↑	↑	↑↑↑	↔	↑↑↑
CPI (W/m^2)	↑↑↑	↑↑	↗	↑↑↑	↔	↑↑↑
CPI-RAP (W/m^2)	↑↑↑	↑↑↑	↑↑↑	↑↑↑	↑	↑↑↑
API	↓↓↓	↔	↓↓	↑↑↑	↓	↑
MPS	↓↓↓	↗	↓	↑↑↑	↔	↑↑↑
Right ventricular function–derived variables						
RAP/PAWP	↓↓↓	↘	↓↓↓	↔	↓↓↓	↓↓↓
PAPI	↑↑↑	↑↑↑	↑↑↑	↑↑↑	↑↑↑	↑↑↑
PVR (dynes·sec·cm^{-5})	↓↓↓	↘	↓↓↓	↑	↓↓↓	↓↓↓
PVRi (dynes·sec·cm^{-5})	↓↓↓	↘	↓↓↓	↑	↓↓↓	↓↓↓
Pulmonary artery compliance	↑↑↑	↑↑	↑↑	↑↑	↑↑↑	↑↑↑
RVSWi (g·m/m^2)	↑↑↑	↑↑	↑↑↑	↑↑	↑↑	↑↑↑
Perfusion pressure variables						
OPP (mm Hg)	↔	↑↑↑	↑↑↑	↑↑↑	↘	↑↑↑
CPP (mm Hg)	↓↓↓	↑↑	↓↓	↑↑↑	↓↓↓	↔
Echocardiographic variables						
LVEF (%)	↑↑↑	↑	↑↑↑	↑↑↑	↑↑	↑↑↑
Tricuspid S´(cm/s)	↑↑↑	↗	↔	↘	↑↑↑	↑↑↑
TAPSE (mm)	↑↑↑	↗	↑↑↑	↑↑	↔	↑↑
VAC RV (TAPSE/sPAP, mm/mm Hg)	↑↑↑	↗	↑↑↑	↑↑↑	↑↑↑	↑↑↑
PV loops						
End-diastolic volume (ml)	↔	↔	↓↓	↑↑	↑	↑↑↑
End-systolic volume (ml)	↘	↔	↓↓↓	↑↑	↑	↑↑
End-systolic pressure (mm Hg)	↓↓↓	↗	↑	↑↑↑	↓↓↓	↔
Arterial elastance (mm Hg/ml)	↓↓↓	↓↓↓	↘	↔	↓↓↓	↓↓↓
End-systolic LV elastance ((R)Ees mm Hg/ml)	↓	↔	↑↑↑	↑	↓↓	↔
LV-VAC	↓↓↓	↘	↓↓↓	↓↓	↔	↓↓↓
SW (mm Hg·ml)	↑↑↑	↑	↑	↑↑↑	↔	↑↑↑
PE (mm Hg·ml)	↓↓↓	↔	↓↓	↑↑↑	↔	↑↑↑
PVA (mm Hg·ml)	↓	↗	↔	↑↑↑	↔	↑↑↑
PVA × HR (mm Hg·ml·bpm)	↓↓	↔	↘	↑↑↑	↔	↑↑↑
Ventricular efficiency (%)	↑↑↑	↑	↑↑↑	↑↑	↑	↑↑↑
α	↑↑↑	↓↓↓	↑↑↑	↓↓↓	↑↑↑	↑↑↑
β	↓↓↓	↑↑↑	↓↓↓	↔	↓↓	↓↓↓
V_0 (ml)	↔	↔	↓↓↓	↑↑↑	↑	↑↑↑
V_{30} (ml)	↓	↔	↓↓↓	↑↑↑	↑	↑↑↑
Other variables						
LVIS	↑	↗	↓↓↓	↓↓↓	↓↓	↗

≥0.95 Very likely positive effect ↑↑↑; 0.90–0.949 likely positive effect ↑↑; 0.80–0.899 probable positive effect ↑; 0.70–0.799 weak positive trend ↗; 0.30–0.699 uncertain/no clear direction ↔; 0.20–0.299 weak negative trend ↘; 0.10–0.199 probable negative effect ↓; 0.05–0.099 likely negative effect ↓↓; ≤0.049 very likely negative effect ↓↓↓; — no data.

α, EDPVR slope (alpha constant); β, EDPVR curvature (beta constant); API, aortic pulsatility index; CO, cardiac output; CPI, cardiac power index; CPI-RAP, CPI adjusted for RAP; CPO, cardiac power output; CPP, coronary perfusion pressure; DBP, diastolic blood pressure; dPAP, diastolic pulmonary artery pressure; Ea, arterial elastance; ESP, end-systolic pressure; Hb, hemoglobin; HCO_3^-, bicarbonate; HR, heart rate; LVEF, left ventricular ejection fraction; LVIS, Levosimendan vasoactive inotropic score; LVSW, left ventricular stroke work; LVSWi, left ventricular stroke work index; MAP, mean arterial pressure; mPAP, mean pulmonary artery pressure; MPS, Myocardial Performance Score; OPP, organ perfusion pressure; PAWP, pulmonary artery wedge pressure; PAPI, pulmonary artery pulsatility index; PE, potential energy; pH, arterial pH; PVA, pressure–volume área; PVR, pulmonary vascular resistance; PVRi, pulmonary vascular resistance index; (R)Ees, end-systolic LV elastance; RAP, right atrial pressure; RAP/PAWP, RAP to PAWP ratio; RVSW, right ventricular stroke work; RVSWi, right ventricular stroke work index; SBP, systolic blood pressure; sPAP, systolic pulmonary artery pressure; SvO_2, central venous oxygen saturation; SV, stroke volume; SVi, stroke volume index; SVR, systemic vascular resistance; SVRi, systemic vascular resistance index; SW, stroke work; TAPSE, tricuspid annular plane systolic excursión; V_0, volume-axis intercept; V_{30}, volume at end-diastolic pressure of 30 mm Hg; VAC, ventricular arterial coupling.

biventricular response, decongestion, and reduced interdependence. These patterns align with reports of improved flow and decongestion in AMI-CS supported with mAFP,[25] although our study was not designed to infer clinical outcomes. These mechanistic findings in ventricular unloading strategies in AMI-CS suggest that active support could be better under low-pressure CS, as seen in DanGer Shock[25,26]; in contrast to normotensive or hypertensive patients without CS, like STEMI-DTU.[27] The reduced API and MPS pattern should be interpreted cautiously; prior studies have reported API improvement during tMCS, including mAFP-supported cohorts undergoing recovery/weaning assessment.[27,28] In contrast, our analysis was not designed around clinical recovery endpoints but around mechanistic PV-surrogate trajectories. Accordingly, the discrepancy may reflect differences in sample size, timing of assessment (<24 h in our study), endpoint definition, and methodology.

Conversely, in HF-CS patients supported with mAFP, responses were less pronounced and heterogeneous in this very small subgroup. Despite modest pressure–flow changes (MAP rose, pulmonary pressures fell), PV surrogates showed no consistent energetic unloading. This signal should not be interpreted as evidence that mAFP worsens ventricular energetics in HF-CS. Rather, it should be viewed as hypothesis-generating and interpreted in the context of prior API-based studies suggesting improvement during temporary support, which our sample size and modeling framework do not allow us to meaningfully confirm or refute.[27,29]

The IABP subgroups showed pulsatile augmentation with modest volume changes. In AMI-CS, IABP lowered pulmonary and left-sided filling pressures while maintaining systemic pressure, with slight improvements in coupling and cardiac power, indicating a pressure-decongestive effect rather than significant unloading.[30] Pressure–volume–derived indices suggested limited shifts in volumes and energetics, with only mild coupling changes. Morici *et al*.[31] also observed this shift in the AMI-CS setting, leading to subtle systolic unloading;[28,32,33] while the absence of a favorable API/MPS profile in our cohort should be interpreted cautiously in light of prior reports of API improvement during temporary support, particularly for assisted API,[34] it should also be noted that our cohort was not analyzed according to clinical responder status or recovery-related clinical endpoints.

In HF-CS, IABP primarily increases pressure and stroke work, suggesting better mechanical output without unloading. The positive API and MPS are directionally consistent with prior work linking API and assisted API to pulsatility and ventriculo-arterial interaction in HF-CS.[28,33,34] These physiologic patterns might help frame the hemodynamic/mechanistic profile with IABP in HF-CS, although interpretation should remain cautious given subgroup size.[35]

In AMI-CS with medical therapy alone, as in DanGer Shock, ischemia-driven recovery showed no improvements in PAP or RAP,[25] alongside afterload relief reflected by lower ESP and effective Ea. Pressure–volume–derived coupling/energetic indices lacked consistent efficiency or unloading signals (SW, PVA, PVA·HR), suggesting the improvement was mainly pressure/afterload-driven. These observations highlight that, in selected AMI-CS, short-term hemodynamic stabilization might occur without tMCS, although the clinical implications require confirmation in larger studies.[36]

In HF-CS without tMCS, medical therapy improved decongestion, forward flow, and LV coupling, with lower PAWP, pulmonary pressures, afterload surrogates, and higher CO/CI and SV. Surrogates such as SW, PVA, and PVA·HR increased, indicating enhanced mechanical output without a reduction in the estimated energy expenditure.[20,21,36] The favorable API/MPS pattern suggests some patients might recover to a more efficient hemodynamic state with medical stabilization alone.[28,33] Overall, these findings are consistent with a pharmacologic "afterload-relief + flow" phenotype.

Limitations

This study has limitations due to small subgroup sizes and variable follow-up intervals, which may affect precision. Pressure–volume–loop metrics estimated indirectly from PAC and echocardiographic data *via* single-beat modeling, including V_0, should be considered physiologic surrogates rather than invasive standards. We did not validate these against conductance-catheter PV loops or consider time-varying therapies. Klotz-derived diastolic indices used PAWP as a surrogate for LVEDP, which may be unreliable with mitral regurgitation, atrial fibrillation, or mechanical ventilation. Pressure–volume area and PVA·HR are modeled surrogates of ventricular energy expenditure, with PVA·HR serving as a global energy proxy. The analysis focuses on short-term hemodynamics and not long-term remodeling or outcomes. Repeated baseline-referenced post-baseline observations were not modeled with random effects or longitudinal covariance, so within-patient dependence and uncertainty may be underestimated.

Conclusions

Bedside derivation of PV-loop surrogates *via* PAC and echocardiography is feasible in CS and may provide complementary physiologic information beyond conventional pressure–flow variables. Observed differences across subgroups, with and without tMCS, should be interpreted as descriptive and exploratory, particularly in the smaller HF-CS subgroups.

Acknowledgments

We thank the cardiology residents, fellows, patients, and families at each site for their support, trust, and participation.

References

1. Bastos MB, Burkhoff D, Maly J, *et al*: Invasive left ventricle pressure–volume analysis: Overview and practical clinical implications. *Eur Heart J* 41: 1286–1297, 2020.
2. Shin WJ, Song JG, Jun IG, *et al*: Effect of ventriculo-arterial coupling on transplant outcomes in cirrhotics: Analysis of pressure-volume curve relations. *J Hepatol* 66: 328–337, 2017.
3. Kataria R, Roswell RO, Bhave NM, *et al*: 2025 concise clinical guidance: An ACC expert consensus statement on the evaluation and management of cardiogenic shock: A report of the American College of Cardiology Solution Set Oversight Committee. *J Am Coll Cardiol* 85: 2025.
4. Baldetti L, Cosenza M, Galdieri C, *et al*: Invasive hemodynamic monitoring in acute heart failure and cardiogenic shock. *Rev Cardiovasc Med* 26: 27034, 2025.
5. Lang RM, Badano LP, Victor MA, *et al*.: Recommendations for cardiac chamber quantification by echocardiography in adults: an update from the American Society of Echocardiography and

the European Association of Cardiovascular Imaging. *J Am Soc Echocardiogr* 28: 1–39.e14, 2015.
6. Arvidsson PM, Berg J, Carlsson M, Arheden H: Noninvasive pressure-volume loops predict major adverse cardiac events in heart failure with reduced ejection fraction. *JACC Adv* 3: 100946, 2024.
7. Fazzini L, Padkins MR, Berg-Hansen K, *et al*: Left ventricular-arterial coupling and mortality in the cardiac intensive care unit. *Eur Heart J Acute Cardiovasc Care* 14: 394–402, 2025.
8. Klotz S, Dickstein ML, Burkhoff D: A computational method of prediction of the end-diastolic pressure-volume relationship by single beat. *Nat Protoc* 2: 2152–2158, 2007.
9. Klotz S, Hay I, Dickstein ML, *et al*: Single-beat estimation of end-diastolic pressure-volume relationship: a novel method with potential for noninvasive application. *Am J Physiol Heart Circ Physiol* 291: H403–H412, 2006.
10. Kremer N, Glocker F, Schaefer S, *et al*: Method for generating right ventricular pressure-volume loops in routine practice. *J Heart Lung Transplant* 45: 273–281, 2025.
11. Monge García MI, Saludes Orduña P, Cecconi M: Understanding arterial load. *Intensive Care Med* 42: 1625–1627, 2016.
12. Chen CH, Fetics B, Nevo E, *et al*: Noninvasive single-beat determination of left ventricular end-systolic elastance in humans. *J Am Coll Cardiol* 38: 2028–2034, 2001.
13. Kelly RP, Ting CT, Yang TM, *et al*: Effective arterial elastance as index of arterial vascular load in humans. *Circulation* 86: 513–521, 1992.
14. Holm H, Magnusson M, Jujić A, Bozec E, Girerd N: How to calculate ventricular–arterial coupling? *Eur J Heart Fail* 24: 600–602, 2022.
15. Hieda M, Goto Y: Cardiac mechanoenergetics in patients with acute myocardial infarction: from pressure-volume loop diagram related to cardiac oxygen consumption. *Heart Fail Clin* 16: 255–269, 2020.
16. Frea S, Gravinese C, Boretto P, *et al*: Comprehensive non-invasive haemodynamic assessment in acute decompensated heart failure-related cardiogenic shock: A step towards echo-dynamics. *Eur Heart J Acute Cardiovasc Care* 13: 646–655, 2024.
17. Soliman-Aboumarie H, Vandenbriele C, Baldetti L, *et al*: Echocardiography for short-term mechanical circulatory support: A trans-Atlantic practical guide. *Eur Heart J Imaging Methods Pract* 3: qyaf067, 2025.
18. Seemann F, Arvidsson P, Nordlund D, *et al*: Noninvasive quantification of pressure-volume loops from brachial pressure and cardiovascular magnetic resonance. *Circ Cardiovasc Imaging* 12: e008493, 2019.
19. Green P, Kodali S, Leon MB, Maurer MS: Echocardiographic assessment of pressure volume relations in heart failure and valvular heart disease: Using imaging to understand physiology. *Minerva Cardioangiol* 59: 375–389, 2011.
20. Meani P, Todaro S, Veronese G, *et al*: Science of left ventricular unloading. *Perfusion (United Kingdom)* 40: 818–831, 2024.
21. Nakata J, Yamamoto T, Saku K, Ikeda Y, Unoki T, Asai K: Mechanical circulatory support in cardiogenic shock. *J Intensive Care* 11: 1–14, 2023.
22. Uriel N, Sayer G, Annamalai S, Kapur NK, Burkhoff D: Mechanical unloading in heart failure. *J Am Coll Cardiol* 72: 569–580, 2018.
23. Curran J, Burkhoff D, Kloner RA: Beyond reperfusion: Acute ventricular unloading and cardioprotection during myocardial infarction. *J Cardiovasc Transl Res* 12: 95–106, 2019.
24. Baldetti L, Busnardo E, Pazzanese V, *et al*: Myocardial viability assessment during Impella support with 18-fluorodesoxyglucose PET imaging. *ESC Heart Fail* 12: 683–687, 2024.
25. Møller JE, Beske RP, Jensen LO, *et al*; DanGer Shock Investigators: Effect of microaxial flow pump on hemodynamics in STEMI-related cardiogenic shock. *J Am Coll Cardiol* 85: 2456–2468, 2025.
26. Møller JE, Engstrøm T, Jensen LO, *et al*: Microaxial flow pump or standard care in infarct-related cardiogenic shock. *N Engl J Med* 390: 1382–1393, 2024.
27. Biscopink A, Moore R, Silkowski M, *et al*: Aortic pulsatility index as a marker of weaning to native recovery in patients supported with an Impella CP for cardiogenic shock. *J Card Fail* 31: 144–148, 2025.
28. Belkin MN, Shah J, Neyestanak ME, Burkhoff D, Grinstein J: Should we be using aortic pulsatility index over cardiac power output in heart failure cardiogenic shock? *Circ Heart Fail* 15: e009601, 2022.
29. Medina ML, Lewin D, Treede H, *et al*: Multicentre comparison of various microaxial pump devices as a bridge to durable assist device implantation. *ESC Heart Fail* 12: 2552–2564, 2552.
30. Kawaguchi O, Pae WE, Daily BB, Pierce WS: Ventriculoarterial coupling with intra-aortic balloon pump in acute ischemic heart failure. *J Thorac Cardiovasc Surg* 117: 164–171, 1999.
31. Morici N, Marini C, Sacco A, *et al*: Intra-aortic balloon pump for acute-on-chronic heart failure complicated by cardiogenic shock. *J Card Fail* 28: 1202–1216, 2022.
32. Thiele H, Zeymer U, Neumann F-J, *et al*; IABP-SHOCK II Trial Investigators: Intraaortic balloon support for myocardial infarction with cardiogenic shock. *N Engl J Med* 367: 1287–1296, 2012.
33. Grinstein J, Belkin MN: Bedside integration of ventricular–arterial coupling, cardiac energetics, and advanced hemodynamics in the management of heart failure. *J Card Fail Intersect* 2: 86–88, 2025.
34. Zainab K, Taylor E, Gangasani N, *et al*: Aortic pulsatility index predicts native recovery in patients with cardiogenic shock supported by intra-aortic balloon pumps. *J Card Fail* 31: 1609–1617, 2025.
35. Morici N, Sacco A, Frea S, *et al*: Early intra-aortic balloon support for heart failure-related cardiogenic shock: A randomized clinical trial. *J Am Coll Cardiol* 85: 1587–1597, 2025.
36. Furer A, Wessler J, Burkhoff D: Hemodynamics of cardiogenic shock. *Interv Cardiol Clin* 6: 359–371, 2017.